



Melt compounding of spray-dried cellulose nanofibrils/polypropylene and their application in 3D printing

Sungjun Hwang · Yousoo Han ·
Douglas J. Gardner

Received: 13 February 2024 / Accepted: 29 June 2024 / Published online: 10 July 2024
© The Author(s) 2024

Abstract Micro- and nano-scale cellulosic fillers exhibit excellent dispersion and distribution within a thermoplastic matrix during the process of melt compounding or injection molding. In this study, spray-dried cellulose nanofiber (SDCNF) powders were manufactured using a pilot-scale rotating disk atomizer spray dryer. Bleached Kraft pulp (BKP), unbleached Kraft pulp (UKP), and old corrugated cardboard pulp (OCC) fibrillated at a fines level of 90% were used as feedstock materials for spray-drying. BKP-, UKP-, and OCC- SDCNFs were compounded with polypropylene using a twin screw co-rotating extruder. Maleic anhydride grafted polypropylene (MAPP) was used as a coupling agent in the composite formulations. The tensile, flexural,

and impact properties of SDCNF-filled PP composites increased at 10 wt% SDCNF loading. The presence of SDCNFs in the PP matrix resulted in faster crystallization and a 12% reduction in the degree of crystallinity of the neat PP. The coefficient of thermal expansion (CTE) of neat PP was reduced by up to 31% attributable to the presence of the SDCNFs. Application of the SDCNF-reinforced PP composites in 3D printing reduced the shrinkage rate of the printed neat PP by 39%, and the printability of the PP was significantly improved with the addition of the SDCNFs.

Keywords 3D printing · Cellulose nanofibrils · Spray-drying · Polypropylene

Supplementary Information The online version contains supplementary material available at <https://doi.org/10.1007/s10570-024-06038-w>.

S. Hwang (✉) · Y. Han (✉) · D. J. Gardner (✉)
Advanced Structures and Composites Center, University of Maine, 35 Flagstaff Road, Orono, ME 04469-5793, USA
e-mail: sungjun.hwang@maine.edu

Y. Han
e-mail: yousoo.han@maine.edu

D. J. Gardner
e-mail: douglasg@maine.edu

S. Hwang · Y. Han · D. J. Gardner
School of Forest Resources, University of Maine, 5755
Nutting Hall, Orono, ME 04469-5755, USA

Introduction

The 3D printing process, also known as additive manufacturing (AM) builds three-dimensional objects by adding materials layer by layer based on a computer-aided design (CAD) model. AM can streamline the production process by eliminating the need for intricate tooling or setups, resulting in time and money savings (Gao et al. 2015). Different types of raw materials including thermoplastics, metal powders, sand, and cement require different AM techniques to create parts (Thompson et al. 2016). For instance, thermoplastics can be printed using fused filament fabrication (FFF) or fused pellet modeling (FPM),

commonly referred to as fused layer modeling (FLM), which is operated using a melt extrusion-based method (Vaes and Van Puyvelde 2021). FLM technology utilizes both filament- and pellet-fed extruders (Shaik et al. 2021). A filament-fed extruder is typically used for a small-scale and desktop 3D printing (Shah et al. 2019). The disadvantage of filament fed extruders is the limited variety of materials available for 3D printing (Moreno Nieto et al. 2018). The quality of filament has a significant impact on the final 3D printed parts, particularly in the case of wood-based reinforced thermoplastic composites (Gardner and Wang 2019). If the wood-based filler absorbs moisture, the moisture penetrates the material and can be trapped inside the filament. The trapped moisture can turn into steam and expand during the extrusion process, reducing the dimensional tolerances and forming a non-circular filament which can negatively affect the quality of the printed parts (Kuboki 2014; Pickering and Stoof 2017). For pellet-fed extruders, the pellets can be added to extruders without a process step of pre-manufactured filaments, resulting in a wider range of materials available for 3D printing and are less expensive than filament fed extruders. Pellets can also be melted and extruded at higher rates with less nozzle clogging than filament fed extruders, making pellet-fed the extruders the standard for large-scale extrusion-based 3D printing (Woern et al. 2018). The pellet-fed big area additive manufacturing (BAAM) 3D printer was developed in 2015 by the Oak Ridge National Lab and Cincinnati Machinery (Love 2015).

Polypropylene (PP) is a widely used commodity semicrystalline thermoplastic that finds applications in various industries such as the automotive, packaging, medical devices, and consumer products attributable to its useful properties of low cost, good processability, resistance to weathering, high impact, and recyclability (Yang et al. 2013; Peltola et al. 2014; Mazzanti et al. 2019). The benefits of PP also contribute to increasing interest in applying PP to FLM technology (Carneiro et al. 2015). However, the high crystallinity and its relatively higher coefficient of thermal expansion (CTE) makes PP prone to the shrinkage or warping of 3D printed parts during crystallization (Savu et al. 2019; Lamm et al. 2020). These material properties limit the applicability of PP in FDM technology compared to other semicrystalline thermoplastics including polylactic acid (PLA)

and acrylonitrile butadiene styrene (ABS) (Fitzharris et al. 2018; Savu et al. 2019). Previous studies have shown that blending PP with other thermoplastics (e.g., polyethylene terephthalate, polyamide 6, polylactic acid, polystyrene) can reduce shrinkage attributable to the increased amorphous regions of PP composites (Chatham et al. 2019; Peng et al. 2019; Choe et al. 2022; Chu et al. 2022). Incorporating inorganic reinforcing fillers including glass, carbon, and talc fibers into PP reduces the shrinkage of the printed parts by increasing the crystallization temperature and thermal conductivity (Spoerk et al. 2018a; Sodeifian et al. 2019; Austermann et al. 2023). Furthermore, smaller sized, spherical shaped fillers including glass spheres and perlite also reduces the warpage of PP attributable to a higher interfacial bonding between the fillers and the matrix. In addition, micro/nano fillers can reduce the degree of crystallinity of PP (Spoerk et al. 2017a, 2018b).

Interest in utilizing natural-based fillers as reinforcement in thermoplastics is increasing attributable to severe environmental concerns (Ho et al. 2012). According to a business data platform (Garside 2023), as of 2022, the global market volume of polypropylene was 79 million metric tons and is expected to increase to 105 million metric tons by 2030. Since PP is not a biodegradable material, using natural-based fillers as reinforcing agents in PP can act as a means to preserve the environment, proportional to the amounts of natural-based fillers used. Previous research has shown that the shrinkage rates of PP can be reduced by adding natural-based fillers including harakeke, hemp, and gypsum, and the reduction in warpage increases as filler contents increase (Stoof and Pickering 2018). However, the issue of filler agglomeration remains a challenge for achieving significant reductions in warpage during 3D printing (Spoerk et al. 2019). Spray-dried cellulose nanofibrils (CNFs), referred to as spray-dried CNF (SDCNF) powder can be a potential alternative as a reinforcing filler in thermoplastics. This is because of their excellent dispersion and distribution in polymer matrices attributable to their small-sized individual particles (Peng et al. 2012a; Wang et al. 2016). The rotary disk atomizer is one of the spray drying techniques, and the primary drying principle involves centrifugal force with a rotating atomizer. This spray dryer is commonly used in various industries including the pharmaceutical, chemical manufacturing, and

food attributable to its scalability, high capacity, and efficient drying capabilities (Huang et al. 2006; Woo et al. 2007; Chegini et al. 2012). According to (Wang et al. 2018b), a 10 wt% SDCNFs reduced the shrinkage of isotactic polypropylene (iPP) by increasing nucleation sites induced by the small and spherical shapes of SDCNFs. In addition, the lower coefficient thermal expansion (CTE) of SDCNFs compared to the PP matrix also reduces the warpage of iPP. However, the warpage test was not evaluated by the 3D printing in Wang's research.

The hydroxyl rich surface of cellulose fibers is incompatible with non-polar polymer matrices. This incompatibility often leads to the clumping of the fibers, resulting from hydrogen bonding among the fibrils during thermoplastic compounding processes (Kalia et al. 2014). Maleic anhydride-grafted polypropylene (MAPP) coupling agent is often used to enhance interfacial bonding between cellulosic materials and the PP matrix. The maleic anhydride functional group from MAPP and hydroxyl groups in cellulose can be cross-linked either through esterification or hydrogen bonding, and the PP tail of MAPP becomes entangled with the molten PP matrix (de Melo et al. 2009).

In this study, cellulose nanofibril (CNF) suspensions were produced using a thermo-mechanical refiner with bleached Kraft pulp (BKP), unbleached Kraft pulp (UKP), and old corrugated cardboard pulp (OCC) as feedstock materials. The CNF suspensions were spray-dried using a rotary disk atomizer to produce SDCNFs, followed by the analysis of the morphological properties and particle size distribution of the resulting SDCNF powders. BKP-, UKP-, and OCC- SDCNF powders were compounded with PP using a twin-co rotating extruder, and a maleic anhydride-grafted polypropylene (MAPP) coupling agent was used in the compounding process. After analyzing the mechanical and rheological properties, as well as thermal analysis of injection molded SDCNF-reinforced PP composites, the filled PP composites were applied to FLM using a pellet-fed 3D printer (Gigabot X) to evaluate the effect of SDCNFs on the warpage and printability behavior of PP. This study focused on determining the effects of utilizing SDCNF powders on the strength characteristics and thermal analysis of a PP matrix, and evaluating how these changes affect printability in 3D printing applications. Lab-scale experiments often provide initial insights into

material behavior and printing feasibility before moving forward to pilot or industrial-scale 3D printing. For example, the University of Maine and Oak Ridge National Laboratory produced a 3D printed 56 m² modular house using a thermoplastic polymer with added cellulosic reinforcing filler, named Bio-Home3D (Robles Poblete et al. 2023; Saavedra-Rojas et al. 2024).

Materials and methods

Cellulose nanofibrils

Bleached Kraft pulp (BKP), unbleached Kraft pulp (UKP), and old corrugated cardboard pulp (OCC) were used to produce cellulose nanofibril (CNF) suspensions as feedstock materials for spray drying. A 3.0 wt% solid content of CNF suspensions was produced by the University of Maine Process Development Center (Bilodeau and Paradis 2018). A thermo-mechanical refiner was used to produce the CNF suspensions, and these suspensions were defibrillated to achieve a fines content of up to 90%. The fines content was measured by a MorFi Compact (TechPap, Grenoble, France) indicates the percentage of fibers in the CNF suspensions shorter than 200 µm in the total fiber count from the refining process. For example, 100% fines content of fines level indicates that all fibers are less than 200 µm in length.

Spray drying

CNF suspensions were spray-dried using a pilot-scale rotary disk atomizer. A 3.0 wt% of CNF suspension was diluted to 1.0 wt% solid content prior to spray drying. The drying conditions for all CNF suspensions were set to an inlet temperature of 240 °C, a bag house temperature of 118 °C, an air fan speed of 86%, a heater capacity of 54%, a pump capacity of 50%, and a disk spinning speed at 30,000 rpm. The outlet temperature was maintained at 248 °C during the spray drying process.

Composite manufacturing

A random copolymer polypropylene (Pro-fax 6525, LyondellBasell, Rotterdam, The Netherlands) was used as the polymer matrix. The coupling agent used

was Maleic anhydride-modified homopolymer polypropylene (MAPP) (Polybond 3200, Lawrenceville, GA, USA). 10 wt% SDCNF-filled PP composites were compounded using a melt co-rotating twin-screw extruder (C. W. Brabender Instruments, South Hackensack, NJ, USA) (Table 1). The extruder was set to a temperature of 180 °C for all 5 heating zones and a speed of 100 rpm, and a two-nozzle die with a nozzle diameter of 2.7 mm was used. The composite extrudates were ground using a granulator (Hellweg MDS 120/150, Hackensack, NJ, USA). A Model #50 “Minijector” injection molder, set at a ram pressure of 2500 psi and a temperature of 200 °C, was used to produce mechanical testing specimens according to ASTM standards: D 638–10 for the tensile test, D 790–10 for the flexural test, and D 256–10 for the notched IZOD impact test, respectively.

3D printing

A pellet fed extrusion-based 3D printer Gigabot X (re:3D, Austin, TX, USA) was used in this research having a nozzle arranged vertically along with a compression screw with three heating zones. The heating zones, numbered 0, 1, and 2, are vertically aligned at the top, middle, and bottom, respectively. For the printed tall hexagon, the temperatures were set to 207 °C, 197 °C, and 187 °C for zones 0, 1, and 2, respectively. The temperature decreases by 10 °C sequentially from zone 0 to the next to prevent the burning of composite pellets. Temperature settings for other printed objects are detailed in Table 2. Simplify 3D software (Simplify 3D, OH, USA) was used to control the 3D printing process. Four different types of objects including a tensile specimen (ASTM D638 Type 1), rectangular, cylinder, and hexagon shapes were printed, and the printing conditions for each type of object are detailed in Table 2. Gorilla (Gorilla Glue Co., OH, USA) duct tape made of butyl rubber was used to improve adhesion between the first layer and the printer bed plate. A skirt was applied to the rectangular object to provide

support for the upper layers during the 3D printing process. A higher printing temperature than that of the melt temperature of the polymer was set to improve the flowability of the molten polymer during printing. Before printing objects, a purging system was utilized to determine the optimal printing temperature. This system operated the screw while the printing head was stationary. For the rectangular, tall hexagon, and cylinder, a temperature of 207 °C was applied. However, for the tensile specimens, a slightly higher temperature of 212 °C was needed. This adjustment is likely attributed to the requirements for smaller-sized objects, which need thinner and smaller deposited layer sizes compared to the other printed objects.

Morphological properties and particle size distribution of SDCNFs

Scanning electron microscopy (SEM) images of SDCNF powders and fractured specimens after the IZOD impact tests were analyzed using a Hitachi Tabletop Microscope SEM TM 3000 (Hitachi High-Technologies Corporation, Tokyo, Japan). The accelerating voltage was set to 15 kV, and the magnification was adjusted automatically.

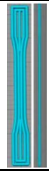
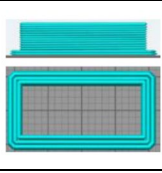
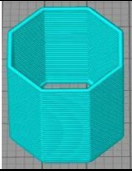

Particle size distribution (PSD) of the powder samples was measured using a Mastersizer 2000 (Malvern Instruments, Worcestershire, United Kingdom). 1 g of each powder sample was measured after being placed on the tray in the Scirocco 2000 attachment (Malvern Instruments, Worcestershire, United Kingdom), with the particle refractive index set at 1.53. In this study, the average particle size of the sample is represented as the surface area [D_{3,2}] value, resulting from a Mastersizer 2000. This is also referred to as Sauter mean diameter, as defined by Eq. (1) (Bellino et al. 2001; Linsinger et al. 2019):

$$d_{3,2} = \frac{1}{\sum_i \frac{p_i}{d_i}} = \frac{6}{\text{specific area}} \quad (1)$$

Table 1 PP SDCNF formulations (wt%)

Composite	Fibrillation level	PP (wt%)	Filler (wt%)	MAPP (wt%)
Neat PP	-	100	0	0
BKP SDCNF-PP	90%	85	10	5
UKP SDCNF-PP	90%	85	10	5
OCC SDCNF-PP	90%	85	10	5

Table 2 3D Printing parameters for the PP SDCNF printed objects

3D printing design model		Tensile specimen	Rectangular	Hexagon	Cylinder
					
Size	X	165 mm	170.87 mm	65.2 mm	65.2 mm
	Y	19 mm	375.59 mm	65.2 mm	65.2 mm
	Z	2.1 mm	92.13 mm	60 mm	60 mm
Temperature	Zone 0	212 °C	207 °C	207 °C	207 °C
	Zone 1	202 °C	197 °C	197 °C	197 °C
	Zone 2	192 °C	187 °C	187 °C	187 °C
Printing speed		6 mm/s	7 mm/s	7 mm/s	7 mm/s
Outline/Perimeter shells		2	1	1	1
Z-Axis Skirt layers/Skirt outlines		2.6 mm	1.8 mm	2.5 mm	2 mm
Outline direction		-	2/2	-	-
Internal infill angle offsets		Outside-in	Outside-in	Outside-in	Outside-in
Interior fill percentage		0°	0°	0°	0°
		0%	0%	0%	0%

d_i : Mean diameter of class i , P_i : Relative volume probability of class i .

High Sensitivity (HS) Circularity and aspect ratios of samples were measured using a Morphologi-G3-ID morphologically directed Raman system (Malvern Instruments, Worcestershire, United Kingdom). A value closer to 1 in HS Circularity is an indicator of a shape that is more circular. The aspect ratio value (width over length) from the Morphologi-G3 is a reciprocal form compared to its commonly accepted interpretation (length over width). The two equations below are the HS Circularity Eq. (2) and aspect ratio Eq. (3) from the Morphologi-G3 analyzer (Ulusoy and Kursun 2011).

$$\text{HS Circularity} = \frac{4\pi \text{Area}}{\text{Perimeter}^2} \quad (2)$$

$$\text{Aspect Ratio} = \frac{\text{Width}}{\text{Length}} \quad (3)$$

Mechanical properties of PP composites

A universal testing machine (Instron 5966) with a 10 kN load cell was used to determine tensile and flexural properties. The tensile strength and tensile modulus of elasticity tests were conducted according to ASTM D638-10 standard (Kwon et al. 2014), and an extensometer was used to measure the elongation of the specimens. The crosshead speed was set at 5 mm/min. Flexural strength and flexural modulus of elasticity tests were performed according to ASTM D790-10 (Appels et al. 2019). Displacement control loading was set to a testing rate of 1.4 mm/min. The applied span was 5.08 mm long for a length/depth ratio of 16. A Ceast pendulum impact tester (Model Resil 50B) was used to measure the Izod impact strength according to ASTM D256-10 (Wang et al. 2018a), and a V-notch was produced on the impact specimens using a Ceast notch cutting machine. Ten impact specimens were tested for each formulation.

Viscoelastic properties of PP composites

The complex viscosity of PP composites was measured using a TA DHR-3 rheometer (TA Instruments, USA). All dynamic experiments were conducted at 207 °C using an 8 mm parallel plate geometry. The rheometer frequency varied from 0.1 to 100 rad/s.

Dynamic mechanical analysis (DMA) was performed using a TA DMA 850 (TA Instruments, USA), and the results were determined using TA TRIOS software. The tests were carried out using a 50 mm three-point bending clamp with a frequency of 1.0 Hz and strain of 0.01%. A temperature range of -30 to 120 °C at a ramp rate of 30 °C/min was used for the DMA testing. A flexural specimen (ASTM D790) was used for the DMA test.

Thermal analysis of PP composites

Differential scanning calorimetry (DSC) tests were conducted using a TA DSC 2500 (TA Instruments, USA), following a sequential heat-cool-heat method. Data analyses were performed using TA TRIOS software. A sample weighing between 5 and 10 mg was sealed in an aluminum pan and subjected to heating from room temperature to 180 °C at a heating rate of 10 °C/min. This process was conducted under a nitrogen atmosphere, with a flow rate of 50 mL/min. The 1st heating scan in the DSC was used to erase the thermal history of the polymer, and the samples were then cooled to -30 °C at a cooling rate of 5 °C/min. The 2nd heating scan was performed up to 180 °C at a heating rate of 10 °C/min, and the degree of crystallinity was calculated from the melting enthalpy of the 2nd heating cycle using Eq. (4) as follows.

$$\% X_{tal} = \frac{\Delta H_m}{\Delta H_m^{\circ}} \times 100\% \quad (4)$$

* ΔH_m : the measured melting enthalpy, ΔH_m° : the reference value for the heat of melting. For polypropylene, this reference value is 207 J/g (Sahin and Yayla 2005; Aljnaid and Banat 2021).

The coefficient of thermal expansion (CTE) was performed using a TMA Q400 (TA Instruments, USA), and the results were determined using TA

Universal Analysis software. The thermomechanical analysis (TMA) samples were cut from the flexural specimens (6.5 mm in length, 4.5 mm in width, and 3.2 mm in thickness). The CTE was measured along the direction of flow in the injection molded samples. The set temperature range was -30 °C to 120 °C at a ramp ratio of 5 °C/min. The CTE of samples was calculated at a temperature range between 25 to 100 °C. Equation (5) used to calculate the CTE is as shown below (James et al. 2001).

$$\alpha = \Delta L / L_0 \Delta T \quad (5)$$

* ΔL is the change in length of the specimen caused by temperature change, L_0 is the length of the specimen at room temperature, ΔT is the change in temperature. Three samples were tested to determine average CTE values.

Measurement of shrinkage and printability of 3D printed parts

The shrinkage of the 3D oriented parts was determined using a tensile specimen Type 1 and a rectangular object. The distances between both curved sides of the printed parts and print bed were measured using Image-J software (Image-J 1.53e, Montgomery, MD, USA) to evaluate the shrinkage rates. The quality of the printed parts was assessed using the printed tall hexagon and cylinder objects.

Statistical analysis

This study utilized JMP Pro 17 (SAS Institute Inc., Cary, NC, USA) for the statistical analysis of polypropylene (PP) composites. The analysis was performed using a one-way ANOVA, followed by the Tukey–Kramer (Honestly Significant Difference) HSD test. The Tukey–Kramer results were presented through a connecting letter report, which identified significantly different groups. The presence of various alphabetical markers on the tables and graphs indicates that each different letter represents a significant difference among groups. Statistical analysis was conducted only if the p-value was less than 0.05.

Results and discussion

Morphological properties and particle size distribution of SDCNFs

Figure 1 shows the SEM images of the 90% fines level of BKP-, UKP- and OCC-SDCNFs. SDCNF powders produced from all feedstock materials were observed as fine powders without fiber clumps. The UKP-SDCNFs contained a higher amount of fibrous material than those of the BKP SDCNFs, and a larger portion of fibrous material was observed in the OCC SDCNFs compared to the UKP SDCNFs. BKP-SDCNFs contained the smallest aspect ratio and highest HS Circularity, followed by the UKP-SDCNFs and OCC-SDCNFs, respectively (Fig. 2). However, the aspect ratio and HS circularity among the BKP-, UKP-, and

OCC-SDCNFs exhibited a similar trend, with circular-shaped powders and low aspect ratio fibrils. These findings are consistent with the results obtained from the SEM images. It can be noted that BKP SDCNFs had the smallest particle size with the narrowest particle size distribution among the feedstock materials (Fig. 3). In general, the BKP pulp contains a higher cellulose content than that of the UKP and OCC pulps resulting from the bleaching treatment on the BKP pulp, resulting in higher refining efficiency (Feijoo et al. 2008). In contrast, the refining efficiency is lower in the UKP and OCC pulps because of higher lignin content in the pulps. Lignin can act as a role of cement between the fibers leading to less separation of the fiber bundles during the refining process (Yook et al. 2020; Copenhaver et al. 2021). During the spray drying process, the bulk liquid, referred to

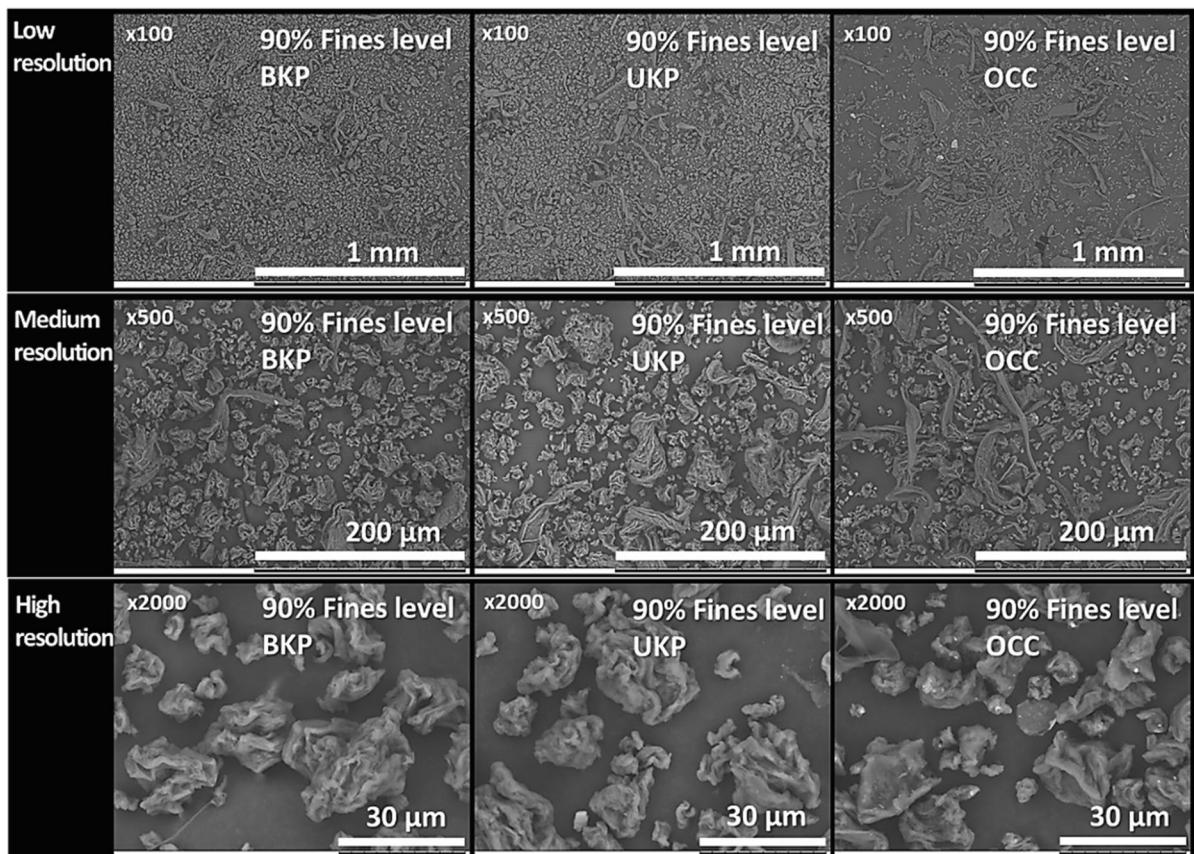
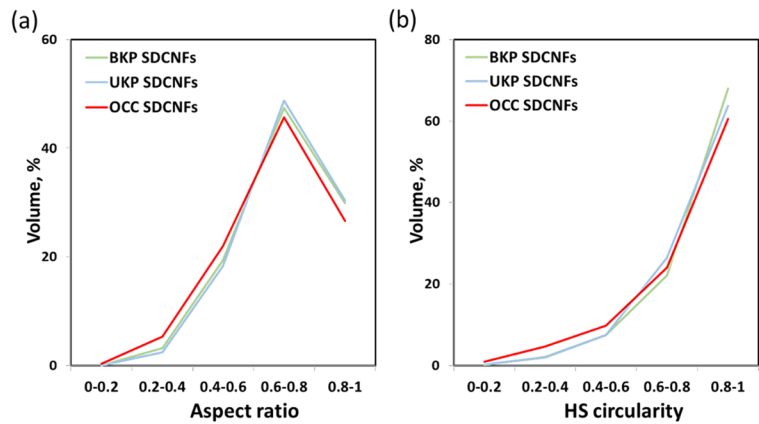


Fig. 1 SEM micrographs (upper: low resolution, middle: medium resolution, bottom: high resolution) of 90% fines level of BKP-, UKP-, OCC-SDCNFs

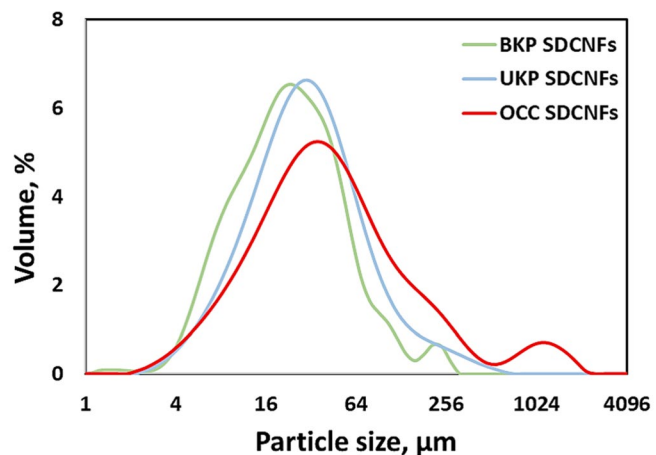
Fig. 2 Aspect ratio (a) and HS circularity (b) of 90% fines level of BKP-, UKP-, OCC-SDCNFs



as "ligaments," is emitted from the rotating atomizer and subsequently broken down into fine droplets. The droplets are exposed to hot air in the drying chamber, causing the water to evaporate. Following the evaporation of water, the remaining cellulose fibrils within the droplets begin to agglomerate, resulting in the formation of particles (Peng et al. 2012b). The less fiber bundles in the BKP-CNF slurry are inserted into the droplets during spray drying, producing smaller particle sizes. Furthermore, the higher repulsive force of the BKP fibrils (-20 mV) compared to that of the OCC fibrils (-8.2 mV) determined from zeta potential analysis can cause them to become distant,

resulting in a smaller number of fibrils being inserted into a droplet during spray-drying, forming smaller individual particles (Cellard et al. 2007; Kelly et al. 2021; Hwang et al. 2023c). In comparison, the OCC SDCNFs exhibited a wider particle size distribution and a higher aspect ratio. This is likely attributed to the inherent properties of the OCC pulp, which tends to become stiff or rigid as a result of the repeated pulping and drying operations in the refining process (Sangtarashani et al. 2020; Lin et al. 2020a). The stiff OCC fibers might form fewer circular shapes, resulting in retaining a larger portion of their fibrous structure (Hwang et al. 2023c).

Fig. 3 Particle size distribution of 90% fines level of BKP-, UKP-, OCC-SDCNFs



	BKP SDCNFs	UKP SDCNFs	OCC SDCNFs
D [3, 2]	14.92	19.14	21.70
d (0.1)	7.12	9.00	9.30
d (0.5)	21.22	27.37	36.02
d (0.9)	59.97	85.96	192.94

The particle size and morphological properties of spray-dried cellulose nanomaterials can vary based on the feedstock and drying conditions, and also, depending on the spray drying technique utilized. In general, there are three different spray drying techniques: the rotary disk atomizer, the two-fluid nozzle, and ultrasonic-assisted spray drying. Smaller-sized droplets can be produced in order from the ultrasonic-assisted spray dryer, two-fluid nozzle, and rotary disk atomizer, producing a size range of droplets from nano- to micrometers. The nanometer spray-dried cellulose nanomaterials dried by an ultrasonic-assisted spray dryer can be applied in many industries, including solvent casting and electrospinning, attributable to their excellent dissolution and distribution in liquid states (Sanders et al. 2023; Hwang et al. 2023a; Dai et al. 2024; Qosim et al. 2024). However, it should be noted that the powder productivity rates might be much lower in the ultrasonic-assisted spray dryer compared to other spray drying techniques attributable to its drying technique. The rotary disk atomizer enables mass production of powders, and this method is easier to scale up to pilot-scale, which leads to the utilization of this spray dryer in 3D printing.

Mechanical properties of PP composites

Table 3 shows the mechanical properties of 10 wt% SDCNF-filled PP composites, demonstrating that the addition of SDCNFs led to improvements in all the mechanical properties of the neat PP. After adding 10 wt% SDCNFs, the tensile strength, tensile modulus of elasticity, flexural strength, and flexural modulus of elasticity of neat PP increased by up to 29%, 66%, 15%, and 27%, respectively. The mechanical properties of the filled PP composites are increased by improving the interfacial bonding between natural filler and PP matrix using the MAPP coupling agent. Larger surface areas with a greater amount of hydroxyl groups on the SDCNF surfaces can bond with PP chains through hydrogen bonding and esterification, resulting from the use of MAPP (Keener et al. 2004; Li et al. 2007; Chun et al. 2015). In addition, the excellent dispersion and distribution of fillers in the PP matrix occurred during the extrusion and injection processes attributable to the small size of the SDCNFs, increased the mechanical properties of neat PP (Soccolingame et al. 2015; Peng et al. 2016; Hwang et al. 2023a, 2024). It appears that the narrower particle size distribution with a larger surface area of BKP- and UKP-SDCNFs than that of

Table 3 Tensile strength and tensile modulus of elasticity, flexural strength and flexural modulus of elasticity, and impact strength of PP composites

Mechanical properties		Neat PP	BKP SDCNF-PP	UKP SDCNF-PP	OCC SDCNF-PP
Tensile strength (MPa)	Average	25.84	33.28	33.21	31.48
	Standard deviation	1.02	0.47	0.36	0.48
	Group*	C	A	A	B
Tensile modulus of elasticity (GPa)	Average	1.22	1.96	2.02	1.72
	Standard deviation	0.12	0.09	0.05	0.06
	Group*	C	A	A	B
Flexural strength (MPa)	Average	47.83	54.58	54.72	54.96
	Standard deviation	1.11	1.29	0.68	1.10
	Group*	B	A	A	A
Flexural modulus of elasticity (GPa)	Average	1.35	1.71	1.71	1.72
	Standard deviation	0.08	0.10	0.03	0.05
	Group*	B	A	A	A
Impact strength (J/m)	Average	34.40	37.88	37.25	31.70
	Standard deviation	6.66	3.17	3.26	3.23
	Group*	AB	A	A	B

*Statistical significance

OCC-SDCNFs leads to a further improvement in the interfacial bonding between the filler and matrix induced by MAPP, resulting in a larger increase in the tensile properties (Dittanet and Pearson 2012; Seydibeyoğlu et al. 2023; Hwang et al. 2024). The lower increase in tensile properties of OCC-SDCNF filled PP composite might be attributable to the higher portion of filler agglomeration attributable to the larger particles' sizes. In general, a higher aspect ratio of individual particles can increase the tensile properties of PP composites; however, there was no difference in aspect ratio values among the different feedstocks in this study. Statistical analysis of the tensile strength and tensile modulus of elasticity supports the results, as determined by statistical significance testing and letter differences from ANOVA and Tukey HSD tests. Neat PP is categorized as group C, while the BKP- and UKP-SDCNF filled PP composites are in group A, and the OCC-SDCNF filled PP composite is in group B. Group C, represented by neat PP, shifted to groups A and B after the addition of SDCNFs. Moreover, group B, of the OCC-SDCNF filled PP composite, exhibits lower tensile properties compared to group A, of the BKP- and UKP-SDCNF filled PP composites. The flexural properties of OCC-SDCNF filled PP composite was similar to BKP- and UKP-SDCNF filled PP composites, and this is likely attributable to the intrinsic stiffness characteristics of OCC fibers from repeated pulping and drying processes in the refining process (Hwang et al. 2023c, 2024). The statistical analysis of the flexural strength and flexural modulus of elasticity was observed with neat PP in group B, and all SDCNF-filled PP composites were categorized as group A. It is worth mentioning that the impact strength of the neat PP increased after adding SDCNFs, except OCC-SDCNFs. A larger particle size with a high aspect ratio of filler can decrease the impact strength of filled composites attributable to the stress concentration resulting from the larger size of the filler, providing crack initiation within the polymer matrix (Hwang et al. 2024). Furthermore, the addition of the coupling agent in the composites restricts polymer mobility and minimizes fiber pull-outs from the matrix, resulting in a further reduction in the impact strength of the filled composites (Feldmann et al. 2016; Thomason and Rudeiros-Fernández 2018; Hwang et al. 2023b). In the statistical analysis of the impact strength, the neat PP is categorized as

group AB, and the BKP- and UKP-SDCNF filled PP composites are in group A, while the OCC-SDCNF filled PP composite is in group B. This shows that the impact strength of neat PP increased after the addition of BKP- and UKP-SDCNFs, while it decreased with the addition of OCC-SDCNFs. It is believed that the smaller-sized SDCNF particles could effectively hinder crack initiation in the PP matrix, leading to higher impact resistance of the PP composites. The impact strength of PP slightly decreased after adding OCC-SDCNFs, and this might be attributable to their larger particle size compared to the BKP- and UKP-SDCNFs. It was confirmed in previous research that the impact strength of the PP composites filled with 10 wt% 100-mesh screened wood flour containing an average particle size of 38 μm , was 16 J/m (Hwang et al. 2024). This value is half of that observed for the OCC-SDCNFs filled PP composite, and the average particle size of the OCC-SDCNFs is 21 μm .

It can be noted that the comparison of the mechanical performance between 5 wt% and 10 wt% SDCNF filler-filled PP composites was performed in our previous research. This research indicated that the mechanical performance of the 10 wt% SDCNF-filled PP composites was higher compared to those with 5 wt% addition. This is likely attributable to increased rates of hydrogen bonding or esterification reactions between the fiber surface and PP chains, induced by MAPP, as the filler content increased. Exceeding 10 wt% might have a negative effect over the benefits, attributable both to the filler agglomeration within the PP matrix, and also, to an increase in the manufacturing cost of the polymer composites. Further discussion regarding the relationship between the morphological and size distribution of SDCNFs and mechanical properties of SDCNF-filled PP composites is presented in detail in our previous research (Hwang et al. 2023a, b, c, 2024).

Rheological and viscoelastic properties of PP composites

Non-Newtonian fluid behavior was observed as shear thinning (pseudoplastic) for all samples (Fig. 4a), the complex viscosity (η^*) decreased as the shear rate increased (Marcovich et al. 2004). The complex viscosity of PP increased with the addition of SDCNFs and MAPP. This is likely attributable to the restricted movement of PP chains resulting from intermolecular

interactions between the filler and matrix (Seo et al. 2022). According to Hwang et al. 2024, the complex viscosity of 10 wt% UKP-SDCNF filled PP was higher by up to 3 times than that of 10 wt% WF addition at 0.1 rad/s. This is likely attributable to the well-distributed and dispersed the smaller-sized SDCNF particles within the PP matrix, and a larger surface area of SDCNFs, forming stronger interactions between the filler and matrix, compared to WF addition (Hanemann 2008; Spoerk et al. 2019).

The storage modulus reflects the elastic behavior of the composite which is related to the stiffness of the polymer composite (Kord et al. 2017). Figure 4b shows a relation between temperature and storage modulus (E') of the PP composites. The storage modulus of the PP composites decreased as the temperature increased, attributable to the softening of the PP composites (Karaduman et al. 2014). It was confirmed that the peak storage modulus of neat PP increased with the addition of reinforcing materials. This is likely attributable to the fact that the restricted mobility of PP chains induced by fillers leads to an

increase in stress transfer between the polymer matrix and the filler at the interface, resulting in an improvement in the stiffness of the composite (Romanzini et al. 2013; Karaduman et al. 2014).

The loss modulus reflects the viscous behavior of the composite, and this can be measured by the energy dissipated as heat by the material during a deformation process (Rezaei et al. 2009). Figure 4c shows the loss modulus (E'') of PP composites as a function of temperature. The loss modulus peaks of filled PP composites at β -transition associated with the glassy-rubbery transition were found to be broader compared to the neat PP. This is likely attributed to the inhibition of the relaxation process within the composites because of a higher number of chain segments with the addition of fillers (Masłowski et al. 2018). Conversely, a faster relaxation process occurred in neat PP by a lower number of chain segments, allowing them to quickly return to their original shapes when the external forces are removed. In addition, the loss modulus curves of the filled PP composite were higher compared to the neat PP. The

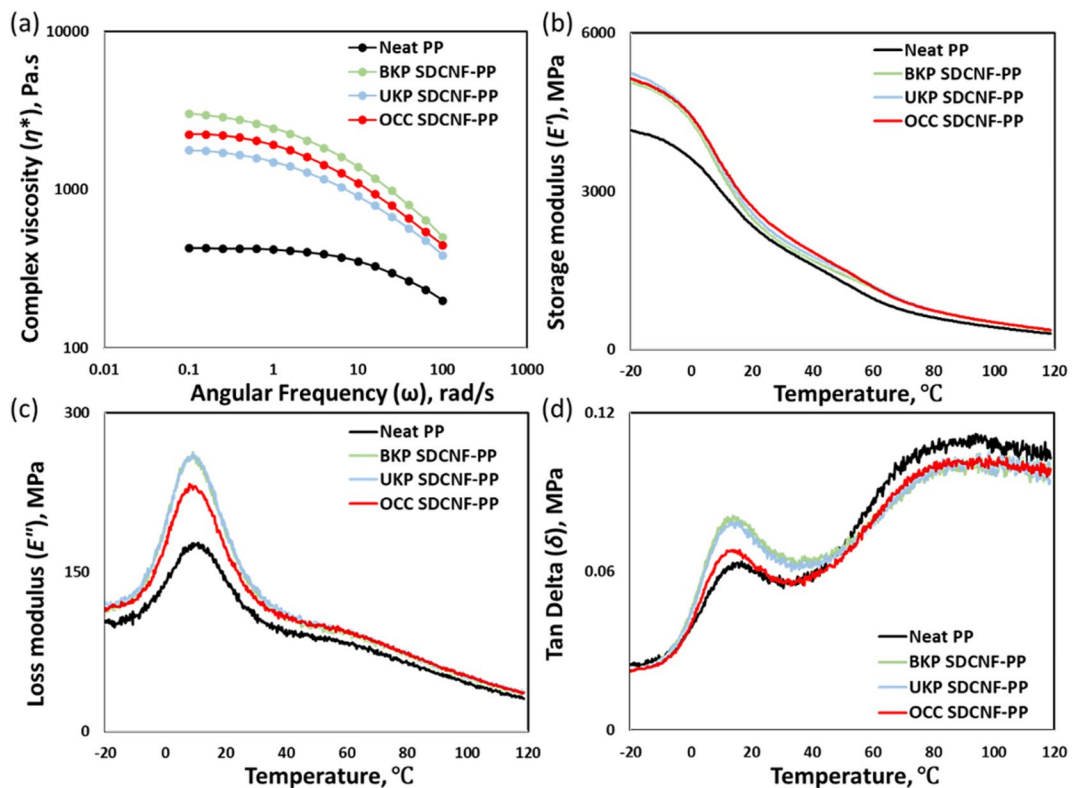


Fig. 4 Complex viscosity (a), storage modulus (b), loss modulus (c), and tan delta (d) of PP composites

reinforcing fillers provide the constraint to the mobilization of the amorphous region of the PP matrix. In other words, the strong formation of chemical bonds between natural filler and PP matrix induced by the MAPP causes the restraint to the molecular motion of polymer near the surface of the fillers. This can create high internal friction at the interface between filler and matrix when external forces are applied, resulting in the high dissipation of energy from the sample (Rajini et al. 2013; Masłowski et al. 2018). The height of the loss modulus above the phase transition region decreases for all samples because of the increased mobility of the polymer chains at high temperatures. It is shown that the BKP- and UKP-SDCNF filled PP composites exhibited a higher and broader peak compared to the OCC-SDCNF filled PP composite. This can be attributed to the further inhibition of the relaxation process and restraint of the molecular motion at the interfaces resulting from a larger surface area of BKP- and UKP-SDCNFs (Ornaghi et al. 2010).

Figure 4d shows the tan delta (δ) as a function of temperature, and this result was consistent with the loss modulus result (Jayanarayanan et al. 2008; Ornaghi et al. 2010; Rajini et al. 2013). The tan delta curves exhibit two characteristic peaks in the vicinity of 10 °C and 100 °C corresponding to the glass transition temperature (T_g) and α -relaxation, respectively (Lee et al. 2009). Below T_g , the molecular chain segments are frozen attributable to insufficient thermal energy to cause the transition. Above T_g , the rotational motion and molecular segments of the chains become free to move and rotate (Jyoti et al. 2016). The shoulder presented on the graph at about 100 °C (α -relaxation) is associated with the crystalline regions of PP chains (Lee et al. 2009). The glass transition temperature (T_g) of neat PP and filled PP composites were measured in the loss modulus and tan delta peaks, and the values are presented in Table 4. It can be anticipated that the addition of filler and coupling agent into polymer matrix can restrict the movement of polymer chains, increasing their T_g (Hidalgo-Salazar and Salinas 2019). In this study, however, the difference of T_g between neat PP and filled PP composites was difficult to find a clear tendency. Previous researchers found that an excessive content of MAPP and the moisture absorption in the wood-based filler can act as plasticizer or lubricant in the polymer

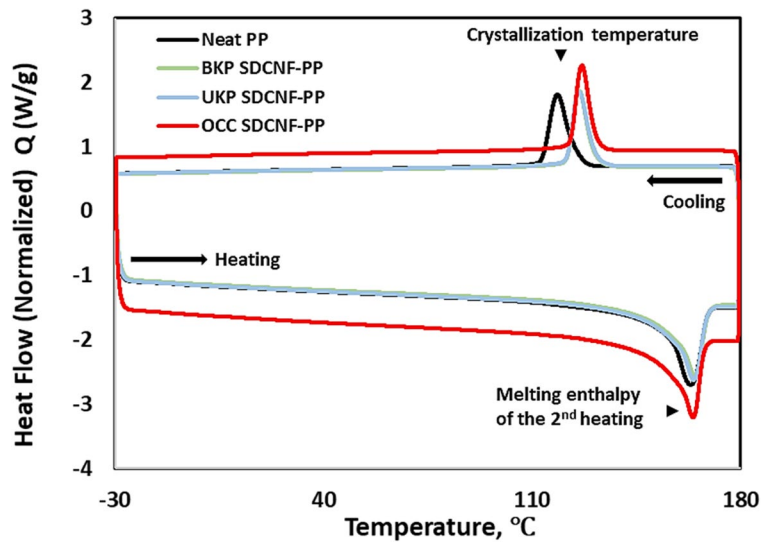
Table 4 Glass transition temperature of PP composites obtained from the loss modulus and tan delta

Samples	Glass transition temperature (T_g)	
	Loss modulus (E'')	Tan delta (δ)
Neat PP	10.74 °C	16.63 °C
BKP SDCNF-PP	8.65 °C	13.43 °C
UKP SDCNF-PP	8.52 °C	15.79 °C
OCC SDCNF-PP	7.42 °C	12.68 °C

composites, increasing the free volume of polymers. This overdose of MAPP and the absorbed moisture in the filler could reduce the glass transition temperatures (Marcovich et al. 1998; Kint et al. 2005; Tajvidi et al. 2006; Wang et al. 2018b). However, the MAPP and wood moisture in this study was not high enough to provide negative impact on the overall performance of the filled PP composites. Other researchers have also found that adding reinforcing fillers, such as nano clay and micrometer-scale date palm fibers, to neat PP composites does not significantly change the glass transition temperature of PP composites (Modesti et al. 2006; Shaikh et al. 2023).

Crystallinity and crystallization temperature of PP composites

Figure 5 shows the DSC graph of 10 wt% SDCNF-filled PP composites. Generally, by incorporating nucleating agents, the crystallization temperature and the degree of crystallinity can be increased, as they promote the growth of crystals within the polymers. In addition, fillers with smaller sizes and larger specific surface area are more effective in enhancing nucleation activity and in accelerating the crystallization temperature. Cellulose fibers and MAPP are known for being effective nucleating agents (Amash and Zugenmaier 1998; Qiu et al. 2003; Lin et al. 2020b). Table 5 shows the crystallization temperature of the PP composites, indicating that the addition of SDCNFs led to an overall increase of 9 °C in the crystallization temperature of neat PP. It is worth nothing that in this study, the addition of SDCNFs resulted in a decrease of up to 12% in the crystallinity degree of neat PP. The incorporation of spherical shaped micron or nano-sized fillers into the polymer matrix can lead

Fig. 5 DSC curves of PP composites**Table 5** Crystallization temperature and crystallinity degree of PP composites

Samples	Crystallization temperature, °C	Crystallinity, %
Neat PP	118	55
BKP SDCNF-PP	126	49
UKP SDCNF-PP	126	50
OCC SDCNF-PP	127	49

to a reduction in the crystallinity degree of polymer composites (Fig. S1). The small sized fillers tend to narrow the gaps between themselves, retarding crystal growth within the confined spaces between the fillers (Fornes and Paul 2003; Gardner and Wang 2019). Moreover, neighboring crystals might impede crystal growth along the fiber axis if a high density of nucleation is generated on each filler surface. During the polymer crystallization process, the highly ordered lamellae transition into spherulites starting from a primary nucleus. The presence of nanofillers induces the formation of a greater number of nuclei, resulting in a smaller sized spherulites with their increased amount. The spherulite growth remains uninterrupted until it encounters an adjacent spherulite, and the presence of neighboring spherulites inhibits further growth (Lorenzo and Müller 2008).

Coefficient of thermal expansion (CTE) of PP composites

Figure 6 shows the thermal expansion of neat PP and filled PP composites as a function of temperature, and the CTE values were calculated based on the thermal expansion curves (Table 6). Overall, the CTE values of the PP was reduced by up to 31% after adding 10 wt% SDCNFs at temperature ranging from 25 to 100 °C. This is likely attributable to the restriction of the thermal expansion resulting from a strong interfacial bonding between the fillers and polymer matrix induced by MAPP. In addition, the CTE values can be lowered by the intrinsically lower CTE of fillers compared to the polymer matrix (Yang et al. 2005; Shaikh et al. 2023). In the statistical analysis, the neat PP in group A shifted to groups AB and B after adding SDCNFs to the PP composites. The same letter was presented in both the UKP- and OCC-SDCNF filled PP composites as group B, and the BKP-SDCNFs filled PP composite was categorized as group AB, as shown in Table 6. The CTE values of filled PP composites were the lowest after adding BKP-SDCNFs into neat PP, compared to UKP- and OCC-SDCNF addition. The difference in CTE values might be depended on the filler size. The average particle size of BKP-, UKP-, and OCC-SDCNFs was 14.95, 19.14, and 21.7 µm, respectively. This trend was also

Fig. 6 Thermal expansion of PP composites

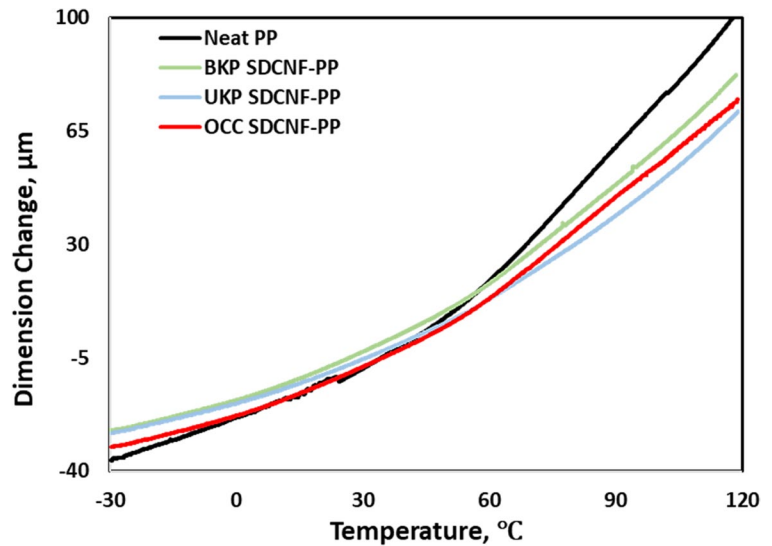


Table 6 Coefficient of thermal expansion (CTE) values of PP composites ranged between 25 to 100 °C

Samples	25 to 100 °C		
	Average CTE (µm/m·°C)	Standard deviation	Group*
PP	169.25	21.43	A
BKP SDCNF-PP	143.15	10.82	AB
UKP SDCNF-PP	122.50	13.00	B
OCC SDCNF-PP	117.07	13.06	B

*Statistical significance

reported by Kim et al. 2007 that the CTE values of rice husk flour (RHF)-reinforced PP composite was lower than WF addition, and the particles size of RHF and WF were ranging from 860 to 270 µm and 110 µm, respectively.

Warpage reduction rates of 3D printed parts

The warpage reduction rates of neat PP and SDCNF-filled PP composites are listed in Table 7, the 3D printed tensile specimen Type 1 and rectangular objects (Figs. 7 and 8). For determining the shrinkage

reduction rate of printed parts, the average distance at which both ends of the tensile specimen and rectangular objects are from the level print bed was measured. The calculated average distances of neat PP were used as a reference, and the reduction rate of printed SDCNF-filled composites was expressed as a percentage relative to this reference value. The maximum shrinkage reduction rates of SDCNF-filled PP composites for all feedstocks were 39.4% and 42.0% in the tensile specimen and rectangular printed parts, respectively, compared to the neat PP. The biggest drawback of the use of PP in 3D printing is the warpage attributable to the higher crystallinity degree and CTE compared to the other thermoplastics including PLA and ABS (Savu et al. 2019). The circular shape with the small size of SDCNFs lowered the crystallinity and CTE of neat PP, reducing the warpage of printed parts (Boschetto and Bottini 2014; Spoerk et al. 2017a; Fitzharris et al. 2018). In addition, Nakashima et al. 1973, reported that the shrinkage in the parallel direction was larger than that in the perpendicular direction. The polymer chains can orient during the flow of the polymer melt, and this causes a difference in the amount of shrinkage in the parallel and perpendicular flow directions. The

Table 7 Shrinkage reduction rates of SDCNF filled PP composites compared to the neat PP

Shrinkage reduction rates, %	BKP SDCNF-PP	UKP SDCNF-PP	OCC SDCNF-PP
Tensile specimen Type I	31.2%	37.1%	39.4%
Rectangular	25.2%	42.0%	37.8%

Fig. 7 3D printed tensile specimens of neat PP and SDCNF filled PP composites

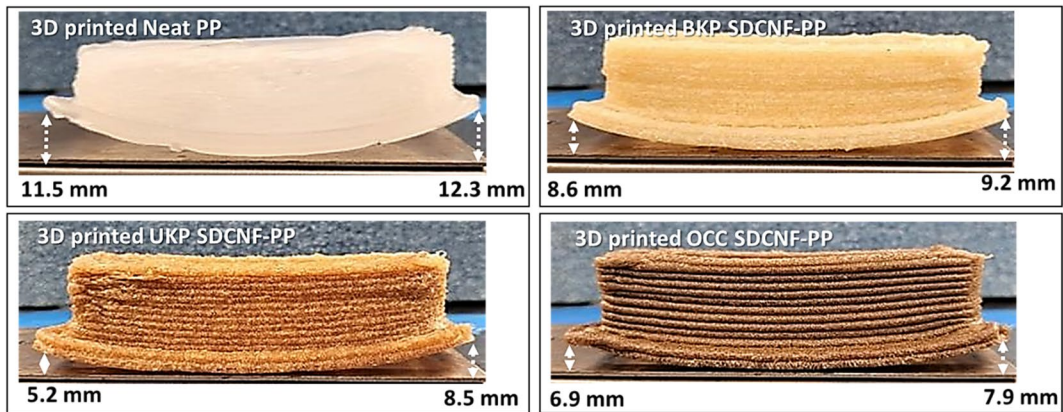
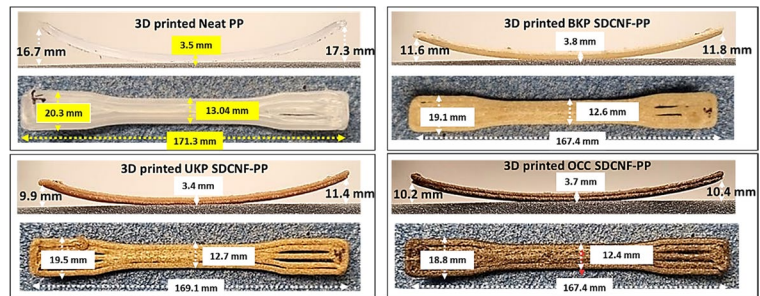


Fig. 8 3D printed rectangular of neat PP and SDCNF filled PP composites

SDCNF might effectively reduce the amount of polymer chain orientation.

The printed tensile specimens were also used to evaluate the dimensional difference of printed parts after 3D printing. The printed tensile specimen of SDCNF-filled PP composites for all feedstocks exhibited a narrower width and shorter length by 5% and 2%, respectively, compared to the neat 3D printed PP (Fig. 7). The low viscosity of PP at higher shear rates leads to the deposition of a thicker layer on the bed plate during 3D printing (Graupner and Müssig 2017). The low viscosity allows the PP to flow more easily, resulting in a higher volume flow rate during the printing process (Fligier et al. 2023). The thick top layer meets the print nozzle, then the molten PP is dragged by the nozzle head, spreading onto the underlying layers (Fig. S2). The addition of SDCNFs into neat PP significantly increases the complex viscosity of composites, resulting in thinner layers being deposited on the plate during printing. This thinner layer prevents contact between the print nozzle and deposited layers during printing. Das et al. 2021 also

reported that excessively low viscosity of molten polymer results in poor resolution of the deposited layers, adversely affecting the shape and dimensional accuracy of the final part.

Printability test of 3D printed parts

Figures 9 and 10 show the 3D printed hexagon and cylinder, respectively, and the two types of objects were used to evaluate the printability test of neat PP and SDCNF-filled PP composites. The printability of neat PP was much lower than that of the filled PP composites and resulted in printing failures after 3D printing for the neat PP. The longer period of molten state of PP on the bed plate might not support the subsequent layers with observed collapsing attributable to the creep phenomenon (Das et al. 2021). As illustrated in Fig. S3, the warpage of printed neat PP can occur during the initial stage of printing, resulting in the deposition of uneven subsequent layers on the bed plate. A gap distance between the print nozzle and the layers can be provided by the uneven

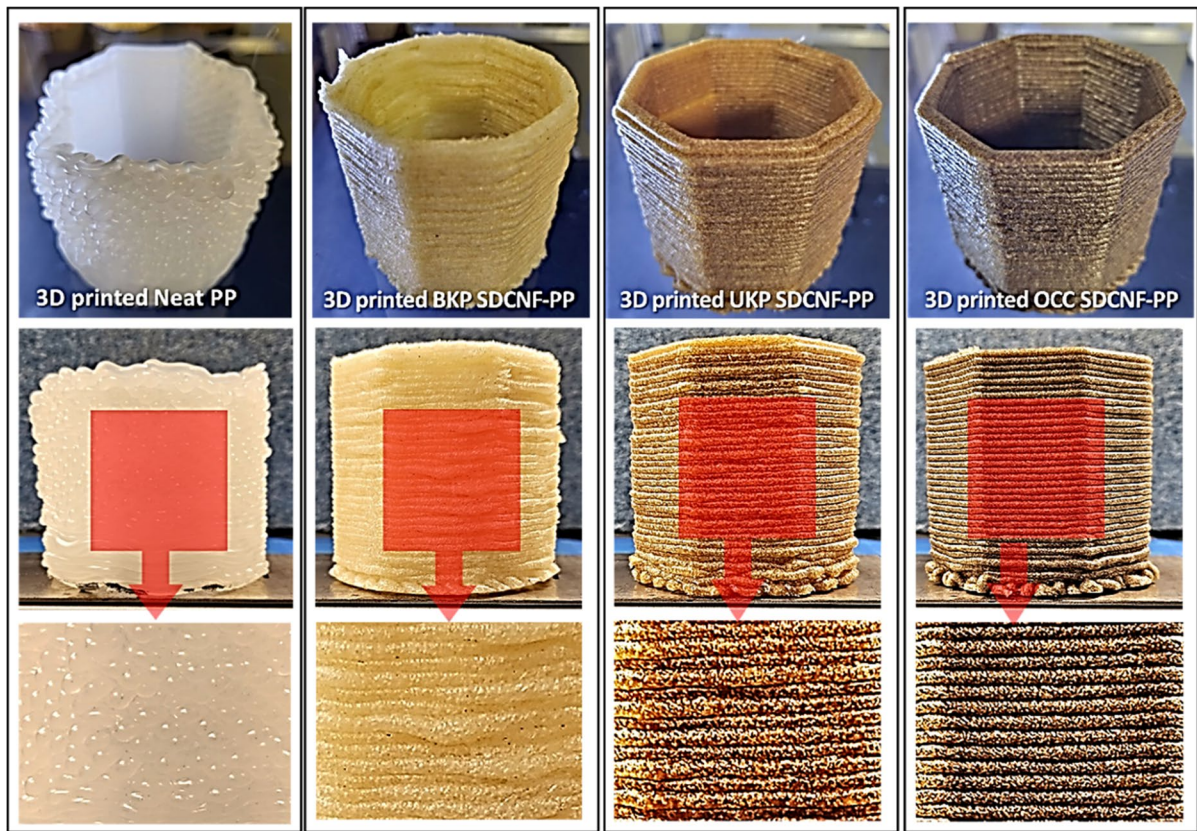


Fig. 9 3D printed hexagon of neat PP and SDCNF filled PP composites and their printability

deposited layer. Over time, this distance continues to increase attributable to the creep phenomenon caused by the molten upper layers. Because of the progressive increase in the gap between the print nozzle and successive layers, the formation of serpentine layers can be deposited on upper layers during printing. In contrast, the distance between the nozzle and the layer was consistent during 3D printing after adding SDCNF powders and MAPP into the neat PP. This is likely attributed to the faster crystallization of PP composites induced by the nucleating agents including SDCNFs and MAPP during the cooling process. The early onset of crystallization prior to the deposition of the strands reduces the molten state time of neat PP (Spoerk et al. 2017b). In addition, the lowered CTE of neat PP by the SDCNF addition can lead to an improvement in the dimensional stability of printed parts at high temperatures, resulting in an increase of printability of printed part (Shaikh et al. 2023). Lastly, the addition of filler increases the

stiffness of the polymer composite, thereby enhancing its resistance to deformation during the printing process. This improved stiffness contributes to the dimensional accuracy of the printed parts (Winter et al. 2022). It can be noted that the printability of BKP-SDCNF filled PP composite was relatively lower than UKP- and OCC-SDCNF filled PP composites, and this is likely attributed to the relatively higher CTE of BKP-SDCNF filled PP composite.

Conclusions

The use of inorganic reinforcing fillers raises environmental concerns, and they can potentially be replaced by natural-based materials. Small sized spray-dried cellulose nanofibril (SDCNF) powders can be promising candidates as a reinforcing material attributable to their sustainability, excellent distribution and dispersion into polymer matrices.

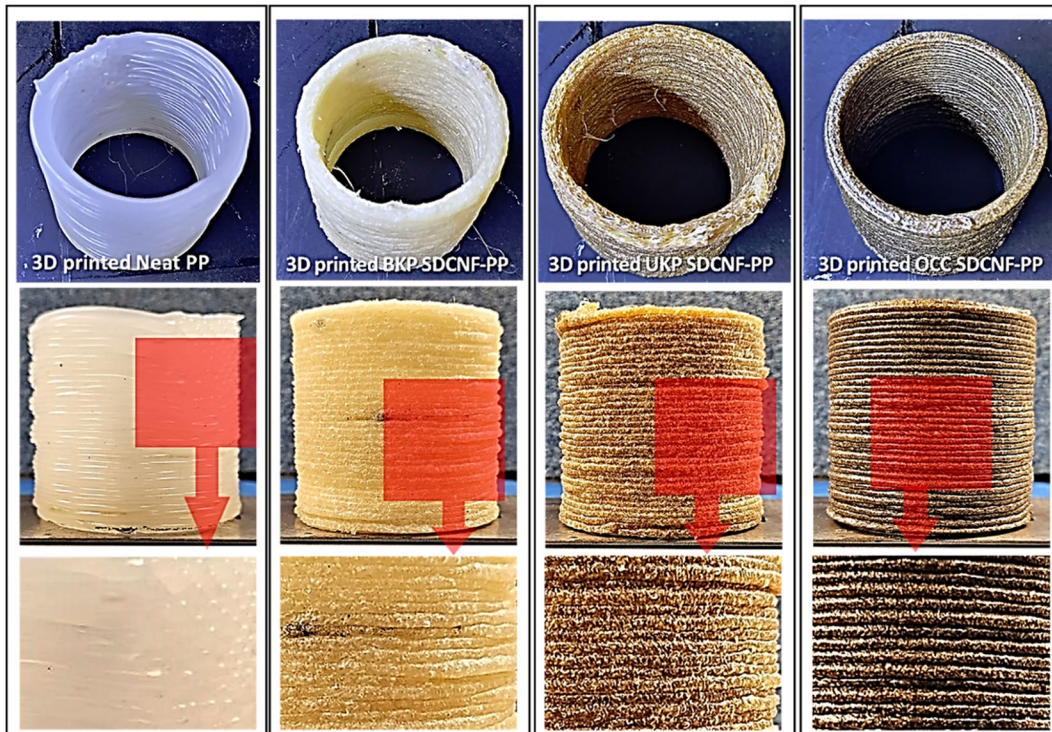


Fig. 10 3D printed cylinder of neat PP and SDCNF filled PP composites and their printability

Furthermore, the small size and spherical shape of SDCNFs, along with their large surface area, enhance interfacial bonding with the PP matrix, which is induced by MAPP. In this work, the effect of spray dried-CNF powders on the material properties of a PP matrix were determined when applied in 3D printing. It was confirmed that SDCNFs contained individual particles less than $20\ \mu\text{m}$ with a spherical shape. The addition of 10 wt% of SDCNFs into neat PP, along with the coupling agent (MAPP), led to a significant enhancement in mechanical properties. The complex viscosity and storage modulus of neat PP increased attributable to the improved interfacial bonding between SDCNFs and the PP matrix induced by MAPP. Furthermore, the addition of SDCNFs into neat PP resulted in a reduction in crystallinity degree by 12% and an increase of $9\ ^\circ\text{C}$ in the crystallization temperature of neat PP. Moreover, the CTE values of SDCNF-filled PP composites decreased by up to 31% because of the intrinsic lower CTE of SDCNFs than that of neat PP. These results improved

warpage reduction rate and printability of neat PP. In this study, a lab-scale pellet type 3D printer was used to assess the potential usage of SDCNFs in 3D printing applications. Future work will expand this lab-scale 3D printing work to pilot-scale with changes in printer nozzle size and printing speed. The microstructure characterization of deposited layers after 3D printing cellulosic materials-filled PP composites, and their effect on the mechanical properties of the printed objects, will be explored in future work.

Acknowledgments This material is based upon work supported by the US Department of Energy (DOE), Office of Energy Efficiency and Renewable Energy, Advanced Materials and Manufacturing Office under CPS Agreement 35863, and Oak Ridge National Laboratory/University of Maine SM2ART program with research and resources used at the Advanced Structures and Composites Center (ASCC), a University of Maine research center. The authors thank the University of Maine Process Development Center (PDC) for producing the CNF suspensions used in this study. Thanks to Jared, trained me on operating the 3D printer, and thanks to Gregory Simms for maintaining the 3D printer for this research.

Author contributions SH conducted the experiments and wrote the main manuscript text. YH and DJG supervised, reviewed, and commented on the manuscript.

Funding US Department of Energy (DOE), Office of Energy Efficiency and Renewable Energy, Advanced Materials and Manufacturing Office under CPS Agreement 35863.

Data availability No datasets were generated or analysed during the current study.

Declarations

Ethics approval and consent to participate Permission to publish is provided by the University of Maine and the research sponsor the US Department of Energy.

Consent for publication All authors have agreed to publish.

Competing interests The authors declare no competing interests.

Open Access This article is licensed under a Creative Commons Attribution 4.0 International License, which permits use, sharing, adaptation, distribution and reproduction in any medium or format, as long as you give appropriate credit to the original author(s) and the source, provide a link to the Creative Commons licence, and indicate if changes were made. The images or other third party material in this article are included in the article's Creative Commons licence, unless indicated otherwise in a credit line to the material. If material is not included in the article's Creative Commons licence and your intended use is not permitted by statutory regulation or exceeds the permitted use, you will need to obtain permission directly from the copyright holder. To view a copy of this licence, visit <http://creativecommons.org/licenses/by/4.0/>.

References

- Aljnaid M, Banat R (2021) Effect of coupling agents on the olive pomace-filled polypropylene composite. *ePolymers* 21:377–390. <https://doi.org/10.1515/epoly-2021-0038>
- Amash A, Zugenmaier P (1998) Study on cellulose and xylan filled polypropylene composites. *Polym Bull* 40:251–258. <https://doi.org/10.1007/s002890050249>
- Appels FVW, Camere S, Montalti M, Karana E, Jasen KMB, Dijksterhuis J, Krijgsheld P, Wösten HAB (2019) Fabrication factors influencing mechanical, moisture- and water-related properties of mycelium-based composites. *Mater Des* 161:64–71. <https://doi.org/10.1016/j.matdes.2018.11.027>
- Austermann J, Kuscera R, Wipperfurth J, Hopmann C, Dahmann R (2023) Influence of material modification and fillers on the dimensional stability and warpage of polypropylene in screw-extrusion-based large area additive manufacturing. *Polym Eng Sci* 63:1598–1612. <https://doi.org/10.1002/pen.26309>
- Bellino I, Bergougnoux L, Misguich-Ripault J, Firpo J-L (2001) Particle size effects on an optical fiber sensor response. *Powder Technol* 115:68–74. [https://doi.org/10.1016/S0032-5910\(00\)00278-3](https://doi.org/10.1016/S0032-5910(00)00278-3)
- Bilodeau MA, Paradis MA (2018) High efficiency production of nanofibrillated cellulose. US Patent No. 9,988,762. <https://patents.google.com/patent/US9988762B2/en>. Accessed 5 Jun 2018
- Boschetto A, Bottini L (2014) Accuracy prediction in fused deposition modeling. *Int J Adv Manuf Technol* 73:913–928. <https://doi.org/10.1007/s00170-014-5886-4>
- Carneiro OS, Silva AF, Gomes R (2015) Fused deposition modeling with polypropylene. *Mater Des* 83:768–776. <https://doi.org/10.1016/j.matdes.2015.06.053>
- Cellard A, Zenati R, Garnier V, Fantozzi G, Baret G (2007) Optimization of chromium oxide nanopowders dispersion for spray-drying. *J Eur Ceram Soc* 27:1017–1021. <https://doi.org/10.1016/j.jeurceramsoc.2006.04.132>
- Chatham CA, Zawaski CE, Bobbitt DC, Moore RB, Long TE, Williams CB (2019) Semi-crystalline polymer blends for material extrusion additive manufacturing printability: a case study with poly(ethylene terephthalate) and polypropylene. *Macromol Mater Eng* 304:1800764. <https://doi.org/10.1002/mame.201800764>
- Chegini GR, Bashiri B, Mesbahi MH (2012) Comparison of pumped air characteristics from a rotary atomizer with three types of wheels. *Exp Tech* 36:63–68. <https://doi.org/10.1111/j.1747-1567.2010.00699.x>
- Choe S, Kim Y, Park G, Lee DH, Park J, Mossisa AT, Lee S, Myung J (2022) Biodegradation of 3D-printed biodegradable/non-biodegradable plastic blends. *ACS Appl Polym Mater* 4:5077–5090. <https://doi.org/10.1021/acscpm.2c00600>
- Chu JS, Koay SC, Chan MY, Choo HL, Ong TK (2022) Recycled plastic filament made from post-consumer expanded polystyrene and polypropylene for fused filament fabrication. *Polym Eng Sci* 62:3786–3795. <https://doi.org/10.1002/pen.26144>
- Chun KS, Husseinsyah S, Osman H (2015) Utilization of cocoa pod husk as filler in polypropylene biocomposites. *J Thermoplast Compos Mater* 28:1507–1521. <https://doi.org/10.1177/0892705713513291>
- Copenhaver K, Li K, Lamm ME, Walker C, Johnson D, Han Y, Wang L, Zhao X, Pu Y, Hinton H, Tekinalp H, Bhagia S, Ragauskas AJ, Gardner DJ, Ozcan S (2021) Recycled cardboard containers as a low-energy source for cellulose nanofibrils and their use in poly(L-lactide). *ACS Sustain Chem Eng* 9:13460–13470. <https://doi.org/10.1021/acssuschemeng.1c03890>
- Dai Y, Sun D, Sundaram S, Delbusso A, Rourke DO, Dorris M, Edirisinghe M (2024) Facile synthesis: from Laminaria hyperborea to cellulose films and fibers. *Cellulose* 31:205–216. <https://doi.org/10.1007/s10570-023-05606-w>
- Das A, Gilmer EL, Biria S, Bortner MJ (2021) Importance of polymer rheology on material extrusion additive manufacturing: correlating process physics to print properties. *ACS Appl Polym Mater* 3:1218–1249. <https://doi.org/10.1021/acscpm.0c01228>
- de Melo JCP, da Silva Filho EC, Santana SAA, Airoidi C (2009) Maleic anhydride incorporated onto cellulose

- and thermodynamics of cation-exchange process at the solid/liquid interface. *Colloids Surf A Physicochem Eng Asp* 346:138–145. <https://doi.org/10.1016/j.colsurfa.2009.06.006>
- Dittanet P, Pearson RA (2012) Effect of silica nanoparticle size on toughening mechanisms of filled epoxy. *Polymer* 53:1890–1905. <https://doi.org/10.1016/j.polymer.2012.02.052>
- Feijoo G, Moreira MT, Álvarez P, Lú-Chau TA, Lema JM (2008) Evaluation of the enzyme manganese peroxidase in an industrial sequence for the lignin oxidation and bleaching of eucalyptus kraft pulp. *J Appl Polym Sci* 109:1319–1327. <https://doi.org/10.1002/app.28084>
- Feldmann M, Heim H-P, Zarges J-C (2016) Influence of the process parameters on the mechanical properties of engineering biocomposites using a twin-screw extruder. *Compos Part A Appl Sci Manuf* 83:113–119. <https://doi.org/10.1016/j.compositesa.2015.03.028>
- Fitzharris ER, Watanabe N, Rosen DW, Shofner ML (2018) Effects of material properties on warpage in fused deposition modeling parts. *Int J Adv Manuf Technol* 95:2059–2070. <https://doi.org/10.1007/s00170-017-1340-8>
- Fligier AW, Rubinić MP, Chmielnicki B (2023) Polypropylene-matrix polymer composites with natural filler. *Arch Metall Mater* 66:313–319. <https://doi.org/10.24425/amm.2021.134789>
- Fornes TD, Paul DR (2003) Crystallization behavior of nylon 6 nanocomposites. *Polymer* 44:3945–3961. [https://doi.org/10.1016/S0032-3861\(03\)00344-6](https://doi.org/10.1016/S0032-3861(03)00344-6)
- Gao W, Zhang Y, Ramanujan D, Ramani K, Chen Y, Williams CB, Wang CCL, Shin YC, Zhang S, Zavattieri PD (2015) The status, challenges, and future of additive manufacturing in engineering. *Comput Aided Des* 69:65–89. <https://doi.org/10.1016/j.cad.2015.04.001>
- Gardner DJ, Wang L (2019) Additive manufacturing of wood-based materials for composite applications. In: proceedings of the SPE automotive composites conference & exhibition. Novi, MI, USA
- Garside M (2023) Polypropylene industry worldwide-statistics & facts. Statista Business data platform. <https://www.statista.com/topics/11793/polypropylene-industry-worldwide>. Accessed 19 Dec 2023
- Graupner N, Müssig J (2017) Cellulose fiber-reinforced PLA versus PP. *Int J Polym Sci* 2017:1–10. <https://doi.org/10.1155/2017/6059183>
- Hanemann T (2008) Influence of particle properties on the viscosity of polymer–alumina composites. *Ceram Int* 34:2099–2105. <https://doi.org/10.1016/j.ceramint.2007.08.007>
- Hidalgo-Salazar MA, Salinas E (2019) Mechanical, thermal, viscoelastic performance and product application of PP-rice husk Colombian biocomposites. *Compos B Eng* 176:107135. <https://doi.org/10.1016/j.compositesb.2019.107135>
- Ho M, Wang H, Lee J-H, Ho C-K, Lau K-T, Leng J, Hui D (2012) Critical factors on manufacturing processes of natural fibre composites. *Compos B Eng* 43:3549–3562. <https://doi.org/10.1016/j.compositesb.2011.10.001>
- Huang LX, Kumar K, Mujumdar AS (2006) A comparative study of a spray dryer with rotary disc atomizer and pressure nozzle using computational fluid dynamic simulations. *Chem Eng Process* 45:461–470. <https://doi.org/10.1016/j.cep.2005.11.004>
- Hwang S, Han Y, Gardner DJ (2024) Morphological characteristics of spray dried cellulose nanofibers produced using various wood pulp feedstocks and their effects on polypropylene composite properties. *Compos B Eng* 268:111093. <https://doi.org/10.1016/j.compositesb.2023.111093>
- Hwang S, Han Y, Gardner DJ (2023a) Characterization of CNC nanoparticles prepared via ultrasonic-assisted spray drying and their application in composite films. *Nanomaterials* 13:2928. <https://doi.org/10.3390/nano13222928>
- Hwang S, Walker CC, Johnson D, Han Y, Gardner DJ (2023b) Spray drying enzyme-treated cellulose nanofibrils. *Polymers* 15:4086. <https://doi.org/10.3390/polym15204086>
- Hwang S, Walker CC, Ozcan S, Tekinalp H, Han Y, Gardner DJ (2023c) Characterization of spray dried cellulose nanofibrils produced by a disk refining process at different fineness levels. *Cellulose* 31:263–277. <https://doi.org/10.1007/s10570-023-05613-x>
- James JD, Spittle JA, Brown SGR, Evans RW (2001) A review of measurement techniques for the thermal expansion coefficient of metals and alloys at elevated temperatures. *Meas Sci Technol* 12:R1–R15. <https://doi.org/10.1088/0957-0233/12/3/201>
- Jayanarayanan K, Thomas S, Joseph K (2008) Morphology, static and dynamic mechanical properties of in situ microfibrillar composites based on polypropylene/poly (ethylene terephthalate) blends. *Compos Part A Appl Sci Manuf* 39:164–175. <https://doi.org/10.1016/j.compositesa.2007.11.008>
- Jyoti J, Singh BP, Arya AK, Dhakate SR (2016) Dynamic mechanical properties of multiwall carbon nanotube reinforced ABS composites and their correlation with entanglement density, adhesion, reinforcement and C factor. *RSC Adv* 6:3997–4006. <https://doi.org/10.1039/C5RA25561A>
- Kalia S, Boufi S, Celli A, Kango S (2014) Nanofibrillated cellulose: surface modification and potential applications. *Colloid Polym Sci* 292:5–31. <https://doi.org/10.1007/s00396-013-3112-9>
- Karaduman Y, Sayeed MMA, Onal L, Rawal A (2014) Viscoelastic properties of surface modified jute fiber/polypropylene nonwoven composites. *Compos B Eng* 67:111–118. <https://doi.org/10.1016/j.compositesb.2014.06.019>
- Keener TJ, Stuart RK, Brown TK (2004) Maleated coupling agents for natural fibre composites. *Compos Part A Appl Sci Manuf* 35:357–362. <https://doi.org/10.1016/j.compositesa.2003.09.014>
- Kelly PV, Gardner DJ, Gramlich WM (2021) Optimizing lignocellulosic nanofibril dimensions and morphology by mechanical refining for enhanced adhesion. *Carbohydr Polym* 273:118566. <https://doi.org/10.1016/j.carbpol.2021.118566>
- Kim H-S, Choi S-W, Lee B-H, Kim S, Kim H-J, Cho CW, Cho D (2007) Thermal properties of bio flour-filled polypropylene bio-composites with different pozzolan contents. *J Therm Anal Calorim* 89:821–827. <https://doi.org/10.1007/s10973-006-7941-3>

- Kint DPR, Seeley G, Gio-Batta M, Burgess AN (2005) Structure and properties of epoxy-based layered silicate nanocomposites. *J Macromol SCI B* 44:1021–1040. <https://doi.org/10.1080/00222340500323656>
- Kord B, Jamshidi M, Hosseinihashemi SK (2017) Effect of multi-walled carbon nanotubes on viscoelastic properties of PP/reed flour composites. *J Polym Environ* 25:1313–1320. <https://doi.org/10.1007/s10924-016-0909-x>
- Kuboki T (2014) Foaming behavior of cellulose fiber-reinforced polypropylene composites in extrusion. *J Cell Plast* 50:113–128. <https://doi.org/10.1177/0021955X13504775>
- Kwon H-J, Sunthornvarabhas J, Park J-W, Lee J-H, Kim H-J, Piyachomkwan K, Sriroth K, Cho D (2014) Tensile properties of kenaf fiber and corn husk flour reinforced poly(lactic acid) hybrid bio-composites: Role of aspect ratio of natural fibers. *Compos B Eng* 56:232–237. <https://doi.org/10.1016/j.compositesb.2013.08.003>
- Lamm ME, Wang L, Kishore V, Tekinalp H, Kunc V, Wang J, Gardner DJ, Ozcan S (2020) Material extrusion additive manufacturing of wood and lignocellulosic filled composites. *Polymers* 12:2115. <https://doi.org/10.3390/polym12092115>
- Lee SH, Kim SY, Youn JR (2009) Effects of maleination and heat treatment on morphology and dynamic mechanical thermal behavior of polypropylene/organoclay nanocomposites. *Compos Part A Appl Sci Manuf* 40:968–974. <https://doi.org/10.1016/j.compositesa.2009.03.013>
- Li X, Tabil LG, Panigrahi S (2007) Chemical treatments of natural fiber for use in natural fiber-reinforced composites: a review. *J Polym Environ* 15:25–33. <https://doi.org/10.1007/s10924-006-0042-3>
- Lin L, Yang J, Ni S, Wang X, Bian H, Dai H (2020a) Resource utilization and ionization modification of waste starch from the recycling process of old corrugated cardboard paper. *J Environ Manage* 271:111031. <https://doi.org/10.1016/j.jenvman.2020.111031>
- Lin Y, Bilotti E, Bastiaansen CWM, Peijs T (2020b) Transparent semi-crystalline polymeric materials and their nanocomposites: a review. *Polym Eng Sci* 60:2351–2376. <https://doi.org/10.1002/pen.25489>
- Linsinger TPJ, Gerganova T, Kestens V, Charoud-Got J (2019) Preparation and characterisation of two polydisperse, non-spherical materials as certified reference materials for particle size distribution by static image analysis and laser diffraction. *Powder Technol* 343:652–661. <https://doi.org/10.1016/j.powtec.2018.11.073>
- Lorenzo AT, Müller AJ (2008) Estimation of the nucleation and crystal growth contributions to the overall crystallization energy barrier. *J Polym Sci B Polym Phys* 46:1478–1487. <https://doi.org/10.1002/polb.21483>
- Love LJ (2015) Utility of big area additive manufacturing (BAAM) for the rapid manufacture of customized electric vehicles. Oak Ridge, TN (United States). Technical Report. <https://doi.org/10.2172/1209199>
- Marcovich NE, Reboredo MM, Aranguren MI (1998) Dependence of the mechanical properties of woodflour-polymer composites on the moisture content. *J Appl Polym Sci* 68:2069–2076. [https://doi.org/10.1002/\(SICI\)1097-4628\(19980627\)68:13%3c2069::AID-APP2%3e3.0.CO;2-A](https://doi.org/10.1002/(SICI)1097-4628(19980627)68:13%3c2069::AID-APP2%3e3.0.CO;2-A)
- Marcovich NE, Reboredo MM, Kenny J, Aranguren MI (2004) Rheology of particle suspensions in viscoelastic media. *Wood flour-polypropylene melt. Rheol Acta* 43:293–303. <https://doi.org/10.1007/s00397-003-0349-0>
- Masłowski M, Miedzianowska J, Strzelec K (2018) Natural rubber composites filled with cereals straw modified with acetic and maleic anhydride: preparation and properties. *J Polym Environ* 26:4141–4157. <https://doi.org/10.1007/s10924-018-1285-5>
- Mazzanti V, Malagutti L, Mollica F (2019) FDM 3D printing of polymers containing natural fillers: a review of their mechanical properties. *Polymers* 11:1094. <https://doi.org/10.3390/polym11071094>
- Modesti M, Lorenzetti A, Bon D, Besco S (2006) Thermal behaviour of compatibilised polypropylene nanocomposite: effect of processing conditions. *Polym Degrad Stab* 91:672–680. <https://doi.org/10.1016/j.polymdegradstab.2005.05.018>
- Moreno Nieto D, Casal López V, Molina SI (2018) Large-format polymeric pellet-based additive manufacturing for the naval industry. *Addit Manuf* 23:79–85. <https://doi.org/10.1016/j.addma.2018.07.012>
- Nakashima K, Fukuta H, Mineki M (1973) Anisotropic shrinkage of injection-molded rubber. *J Appl Polym Sci* 17:769–778. <https://doi.org/10.1002/app.1973.070170309>
- Ornaghi HL, Bolner AS, Fiorio R, Zattera AJ, Amico SC (2010) Mechanical and dynamic mechanical analysis of hybrid composites molded by resin transfer molding. *J Appl Polym Sci* 118:887–896. <https://doi.org/10.1002/app.32388>
- Peltola H, Pääkkönen E, Jetsu P, Heinemann S (2014) Wood based PLA and PP composites: effect of fibre type and matrix polymer on fibre morphology, dispersion and composite properties. *Compos Part A Appl Sci Manuf* 61:13–22. <https://doi.org/10.1016/j.compositesa.2014.02.002>
- Peng X, He H, Jia Y, Liu H, Geng Y, Huang B, Luo C (2019) Shape memory effect of three-dimensional printed products based on polypropylene/nylon 6 alloy. *J Mater Sci* 54:9235–9246. <https://doi.org/10.1007/s10853-019-03366-2>
- Peng Y, Gallegos SA, Gardner DJ, Han Y, Cai Z (2016) Maleic anhydride polypropylene modified cellulose nanofibril polypropylene nanocomposites with enhanced impact strength. *Polym Compos* 37:782–793. <https://doi.org/10.1002/pc.23235>
- Peng Y, Gardner DJ, Han Y (2012a) Drying cellulose nanofibrils: in search of a suitable method. *Cellulose* 19:91–102. <https://doi.org/10.1007/s10570-011-9630-z>
- Peng Y, Han Y, Gardner DJ (2012b) Spray drying cellulose nanofibrils: effect of drying process parameters on particle morphology and size distribution. *Wood Fiber Sci* 44:448–461
- Pickering K, Stoof D (2017) Sustainable composite fused deposition modelling filament using post-consumer recycled polypropylene. *J Compos Sci* 1:17. <https://doi.org/10.3390/jcs1020017>
- Qiu W, Zhang F, Endo T, Hirotsu T (2003) Preparation and characteristics of composites of high-crystalline cellulose with polypropylene: Effects of maleated polypropylene

- and cellulose content. *J Appl Polym Sci* 87:337–345. <https://doi.org/10.1002/app.11446>
- Qosim N, Majd H, Ahmed J, Williams G, Edirisinghe M (2024) Making fibers from cellulose derivatives by pressurized gyration and electrospinning. *Cellulose* 31:2815–2832. <https://doi.org/10.1007/s10570-024-05793-0>
- Rajini N, Jappes JW, Jeyaraj P, Rajakarunakaran S, Bennet C (2013) Effect of montmorillonite nanoclay on temperature dependence mechanical properties of naturally woven coconut sheath/polyester composite. *J Reinf Plast Compos* 32:811–822. <https://doi.org/10.1177/0731684413475721>
- Rezaei F, Yunus R, Ibrahim NA (2009) Effect of fiber length on thermomechanical properties of short carbon fiber reinforced polypropylene composites. *Mater Des* 30:260–263. <https://doi.org/10.1016/j.matdes.2008.05.005>
- Robles Poblete F, Ireland M, Slattery L, Davids WG, Lopez-Anido RA (2023) In situ, real-time temperature mapping and thermal FE simulations of large-format 3D printed PETG/CF vertical wall. *Materials* 16:6486. <https://doi.org/10.3390/ma16196486>
- Romanzini D, Lavoratti A, Ornaghi HL, Amico SC, Zattera AJ (2013) Influence of fiber content on the mechanical and dynamic mechanical properties of glass/ramie polymer composites. *Mater Des* 47:9–15. <https://doi.org/10.1016/j.matdes.2012.12.029>
- Saavedra-Rojas FA, Bhandari S, Lopez-Anido RA (2024) Environmental durability of bio-based and synthetic thermoplastic composites in large-format additive manufacturing. *Polymers* 16:787. <https://doi.org/10.3390/polym16060787>
- Sahin S, Yayla P (2005) Effects of processing parameters on the mechanical properties of polypropylene random copolymer. *Polym Test* 24:1012–1021. <https://doi.org/10.1016/j.polymertesting.2005.07.010>
- Sanders JE, Wang L, Brinkley G, Gardner DJ (2023) Production of nano-scale cellulose nanocrystal powder via electrospray drying (ESD) for sustainable composites. *Cellulose* 30:6303–6315. <https://doi.org/10.1007/s10570-023-05217-5>
- Sangtarashani SMH, Rahmaninia M, Behrooz R, Khosravani A (2020) Lignocellulosic hydrogel from recycled old corrugated container resources using ionic liquid as a green solvent. *J Environ Manage* 270:110853. <https://doi.org/10.1016/j.jenvman.2020.110853>
- Savu ID, Savu SV, Simion D, Sirbu N, Coirnei M, Ratiu SA (2019) PP in 3D printing - technical and economic aspects. *Mater Plast* 56:931–936. <https://doi.org/10.37358/MP.19.4.5286>
- Seo HY, Cho KY, Im D, Kwon YJ, Shon M, Baek KY, Yoon HG (2022) H mechanical properties of covalently functionalized carbon fiber and polypropylene composites by enhanced interfacial adhesion derived from rationally designed polymer compatibilizers. *Compos B Eng* 228:109439. <https://doi.org/10.1016/j.compositesb.2021.109439>
- Seydibeyoğlu MÖ, Dogru A, Wang J, Rencheck M, Han Y, Wang L, Seydibeyoğlu EA, Zhao X, Ong K, Shatkin JA, Es-Haghi SS, Bhandari S, Ozcan S, Gardner DJ (2023) Review on hybrid reinforced polymer matrix composites with nanocellulose, nanomaterials, and other fibers. *Polymers* 15:984. <https://doi.org/10.3390/polym15040984>
- Shah J, Snider B, Clarke T, Kozutsky S, Lacki M, Hosseini A (2019) Large-scale 3D printers for additive manufacturing: design considerations and challenges. *J Adv Manuf Technol* 104:3679–3693. <https://doi.org/10.1007/s00170-019-04074-6>
- Shaik YP, Schuster J, Shaik A (2021) A Scientific review on various pellet extruders used in 3D printing FDM processes. *Oalib* 08:e7698. <https://doi.org/10.4236/oalib.1107698>
- Shaikh H, Alothman OY, Alshammari BA, Jawaid M (2023) Dynamic and thermo-mechanical properties of polypropylene reinforced with date palm nano filler. *J King Saud Univ Sci* 35:102561. <https://doi.org/10.1016/j.jksus.2023.102561>
- Soccalingame L, Bourmaud A, Perrin D, Bénézet J-C, Bergeret A (2015) Reprocessing of wood flour reinforced polypropylene composites: Impact of particle size and coupling agent on composite and particle properties. *Polym Degrad Stab* 113:72–85. <https://doi.org/10.1016/j.polymdegradstab.2015.01.020>
- Sodeifian G, Ghaseminejad S, Yousefi AA (2019) Preparation of polypropylene/short glass fiber composite as fused deposition modeling (FDM) filament. *Results Phys* 12:205–222. <https://doi.org/10.1016/j.rinp.2018.11.065>
- Spoerk M, Arbeiter F, Raguž I, Weingrill G, Fischinger T, Traxler G, Schuschnigg S, Cardon L, Holzer C (2018a) Polypropylene filled with glass spheres in extrusion-based additive manufacturing: effect of filler size and printing chamber temperature. *Macromol Mater Eng* 303:1800179. <https://doi.org/10.1002/mame.201800179>
- Spoerk M, Sapkota J, Weingrill G, Fischinger T, Arbeiter F, Holzer C (2017a) Shrinkage and warpage optimization of expanded-perlite-filled polypropylene composites in extrusion-based additive manufacturing. *Macromol Mater Eng* 302:1700143. <https://doi.org/10.1002/mame.201700143>
- Spoerk M, Savandaiah C, Arbeiter F, Schuschnigg S, Holzer C (2017b) Properties of glass filled polypropylene for fused filament fabrication. In: *SPE ANTEC Anaheim*. California, USA, pp 105–111
- Spoerk M, Savandaiah C, Arbeiter F, Traxler G, Cardon L, Holzer C, Sapkota J (2018b) Anisotropic properties of oriented short carbon fibre filled polypropylene parts fabricated by extrusion-based additive manufacturing. *Compos Part A Appl Sci Manuf* 113:95–104. <https://doi.org/10.1016/j.compositesa.2018.06.018>
- Spoerk M, Savandaiah C, Arbeiter F, Sapkota J, Holzer C (2019) Optimization of mechanical properties of glass-spheres-filled polypropylene composites for extrusion-based additive manufacturing. *Polym Compos* 40:638–651. <https://doi.org/10.1002/pc.24701>
- Stoof D, Pickering K (2018) Sustainable composite fused deposition modelling filament using recycled pre-consumer polypropylene. *Compos B Eng* 135:110–118. <https://doi.org/10.1016/j.compositesb.2017.10.005>
- Tajvidi M, Falk RH, Hermanson JC (2006) Effect of natural fibers on thermal and mechanical properties of natural fiber polypropylene composites studied by dynamic mechanical analysis. *J Appl Polym Sci* 101:4341–4349. <https://doi.org/10.1002/app.24289>

- Thomason JL, Rudeiros-Fernández JL (2018) A review of the impact performance of natural fiber thermoplastic composites. *Front Mater* 5:1–18. <https://doi.org/10.3389/fmats.2018.00060>
- Thompson MK, Moroni G, Vaneker T, Fadel G, Campbell RI, Gibson I, Bernard A, Schulz J, Graf P, Ahuja B, Martina F (2016) Design for additive manufacturing: trends, opportunities, considerations, and constraints. *CIRP Ann* 65:737–760. <https://doi.org/10.1016/j.cirp.2016.05.004>
- Ulusoy U, Kursun I (2011) Comparison of different 2D image analysis measurement techniques for the shape of talc particles produced by different media milling. *Miner Eng* 24:91–97. <https://doi.org/10.1016/j.mineng.2010.05.011>
- Vaes D, Van Puyvelde P (2021) Semi-crystalline feedstock for filament-based 3D printing of polymers. *Prog Polym Sci* 118:101411. <https://doi.org/10.1016/j.progpolymsci.2021.101411>
- Wang L, Kiziltas A, Mielewski DF, Lee EC, Gardner DJ (2018a) Closed-loop recycling of polyamide12 powder from selective laser sintering into sustainable composites. *J Clean Prod* 195:765–772. <https://doi.org/10.1016/j.jclepro.2018.05.235>
- Wang L, Roach AW, Gardner DJ, Han Y (2018b) Mechanisms contributing to mechanical property changes in composites of polypropylene reinforced with spray-dried cellulose nanofibrils. *Cellulose* 25:439–448. <https://doi.org/10.1007/s10570-017-1556-7>
- Wang L, Sanders JE, Gardner DG, Han Y (2016) In-situ modification of cellulose nanofibrils by organosilanes during spray drying. *Ind Crops Prod* 93:129–135. <https://doi.org/10.1016/j.indcrop.2016.02.004>
- Winter K, Wilfert J, Häupler B, Erlmann J, Altstädt V (2022) Large scale 3D printing: influence of fillers on warp deformation and on mechanical properties of printed polypropylene components. *Macromol Mater Eng* 307:2100528. <https://doi.org/10.1002/mame.202100528>
- Woern A, Byard D, Oakley RB, Fiedler MJ, Snabes SL, Pearce JM (2018) Fused particle fabrication 3-D printing: recycled materials' optimization and mechanical properties. *Materials* 11:1413. <https://doi.org/10.3390/ma11081413>
- Woo MW, Daud WRW, Tasirin SM, Talib MZM (2007) Optimization of the spray drying operating parameters—a quick trial-and-error method. *Dry Technol* 25:1741–1747. <https://doi.org/10.1080/07373930701591093>
- Yang H-S, Kiziltas A, Gardner DJ (2013) Thermal analysis and crystallinity study of cellulose nanofibril-filled polypropylene composites. *J Therm Anal Calorim* 113:673–682. <https://doi.org/10.1007/s10973-012-2770-z>
- Yang H-S, Wolcott MP, Kim H-S, Kim H-J (2005) Thermal properties of lignocellulosic filler-thermoplastic polymer bio-composites. *J Therm Anal Calorim* 82:157–160. <https://doi.org/10.1007/s10973-005-0857-5>
- Yook S, Park H, Park H, Lee S-Y, Kwon J, Youn HJ (2020) Barrier coatings with various types of cellulose nanofibrils and their barrier properties. *Cellulose* 27:4509–4523. <https://doi.org/10.1007/s10570-020-03061-5>

Publisher's Note Springer Nature remains neutral with regard to jurisdictional claims in published maps and institutional affiliations.